Thin Maglev Ventricular Assist Device with Radial Type Self-bearing Motor

Michiko Murakami[a], Toru Masuzawa[a], Shoichi Yoshida[a], Hiroyuki Onuma[b],Takashi Nishimura[c], Syunei Kyo[c]

[a] College of Engineering, Ibaraki University, 4-12-1 Nakanarusawa, Hitachi, Ibaraki 316-8511, Japan, 12nd214y@hcs.ibaraki.ac.jp
[b] Department of Electronics and Control Engineering, Ibaraki National College of Technology, 866 Nakane, Hitachinaka, Ibaraki 312-8508, Japan,
[c] Therapeutic Strategy for Heart Failure, the University of Tokyo, 7-3-1 Hongo, Bunkyo, Tokyo,113-8655

***Abstract*— A small, thin, maglev ventricular assist device, which can be implanted under the thorax muscle layer like a pacemaker, has been developed. A cascade pump, which has inlet and outlet ports in the same plane and a radial type self-bearing motor are adopted to reduce the axial thickness of the device. The radial self-bearing motor is using the passive stability to restrict the impeller movement in the axial direction and its inclination. We evaluated the fluid force acted on the levitated impeller by using the computational fluid dynamics analysis and restoring force and torque by using the magnetic field analysis. Also, an axial hydrodynamic bearing is developed to avoid the impeller contact on the casing when the levitated impeller received a large disturbance. Finally, a prototype pump is developed and evaluated its levitation and pump performance. The prototype pump was levitated and rotated up to a rotating speed of 2,600 rpm successfully. The target performance of a flow rate of 2 L/min against a head pressure of 100 mmHg is achieved with a rotating speed of 2,000 rpm. The maximum oscillation amplitude and the total power consumption with the target performance were 17 µm and 4.5 watts.**

I. INTRODUCTION

Ventricular assist device (VAD) is applied for severe heart failure patient [1]. But, intended patients are limited the most severe type because of its high cost. We have been developing a thin maglev VAD with a high reliability, a good cost performance and a long-term usage with periodical replacement. Proposed VAD can be implanted under the thorax muscle layer like a pacemaker by adopting a magnetically levitated cascade blood pump [2] with a radial type self-bearing motor which has an advantage it can be made thinner than axially suspension motor [3]. The cascade pump which has inlet and outlet ports in the same plane is able to reduce the axial thickness of the device. The radial self-bearing motor is using the passive stability to restrict the impeller movement in the axial direction and its inclination to reduce complexity of the magnetic suspension system. In this paper, we evaluated the fluid force acted on the levitated impeller by using the computational fluid dynamics (CFD) analysis and restoring force and torque by using the magnetic field analysis. Also, an axial hydrodynamic bearing was developed to avoid the impeller contact on the casing when the impeller received a large disturbance. Finally, a prototype pump was developed. The basic levitation and pump performance of the prototype pump was evaluated.

II. METHOD

A. *Magnetically levitated cascade blood pump and Self-bearing motor*

Fig. 1 shows a schematic of the magnetically levitated cascade blood pump. Magnetic suspension techniques have been used to eliminate the mechanical contact parts for improvement of device durability. The self-bearing motor is set at the center of the device and the ring-shaped levitated impeller is set at the circumferential space. There is a cylindrical sensor target for the radial position detection on the outer periphery of the levitated impeller. The hydrodynamic bearing is formed on the rotor yoke's end face of the levitated impeller. The target pump performance is a flow rate of 2 L/min against a head pressure of 100 mmHg to assist a part of the cardiac function of patients with mild heart failure. Fig. 2 shows an oblique perspective figure of the radial type self-bearing motor. The outer rotor structure, that a rotor is set around a stator, is adopted to miniaturize the self-bearing motor. Eight thin permanent magnets are set on the inner circumferential surface of the rotor which is a yoke itself. The stator has twelve radial poles. Rotation coils to produce 3-phase 8-pole magnetic field and levitation coils to produce 2-phase 6-pole magnetic field are wound separately on the centered stator yoke. The plus minus two-pole algorithm is adopted to levitate and rotate the rotor. Two radial degrees of freedom of the rotor and rotation of the rotor are controlled actively by electromagnets constructed on the stator. The axial movement and the inclination of the levitated impeller are restricted with the passive stability to reduce complexity of the magnetic suspension system.

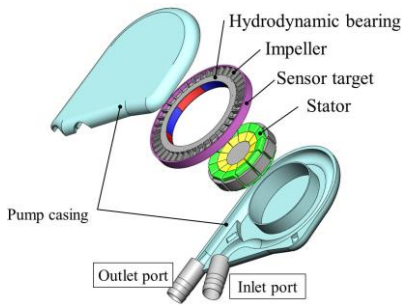

Figure 1. Schematic of the magnetically levitated cascade pump.

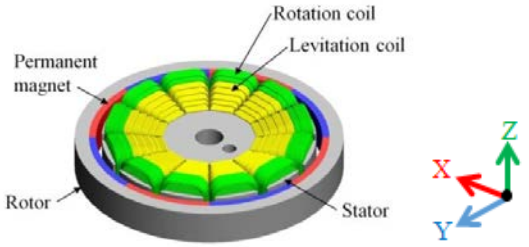

Figure 2. Oblique perspective figure of radial type self-bearing motor.

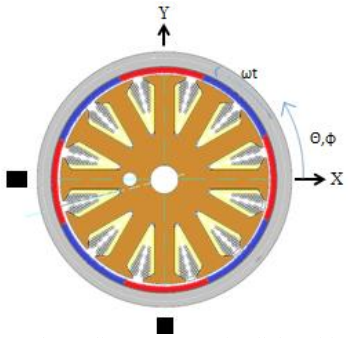

Figure 3. Schematic and coordinate system of radial position control's principle.

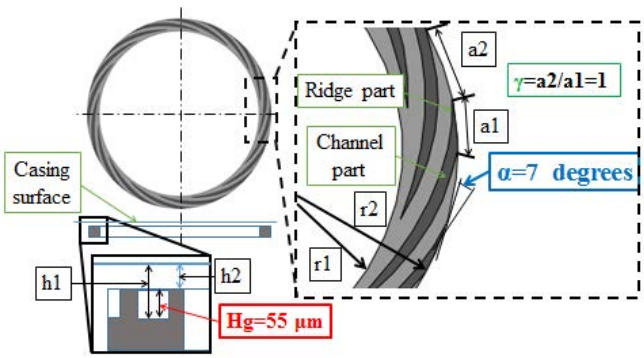

Figure 4. Schematic of the hydrodynamic bearing.

B. *Principle of radial position control*

Fig. 3 shows the schematic and coordinate system of this principle. The permanent magnets of the rotor and the stator are assumed to produce the following magnet flux density B_r (θ, t) and B_s (θ, t),

$$B_r(\theta,t) = B_R \cos(\omega t - M\theta) \quad (1)$$

$$B_s(\theta,t) = B_S \cos(\omega t - N\theta - \phi) \quad (2)$$

where B_R, B_S are peak density of magnetic flux produced by the rotor permanent magnets and the stator electromagnets, M is pole pair number of the rotor, θ is angular coordinate, and ϕ is an arbitrary angle. The magnet flux density of the air gap B_{rs} is sum of the flux density B_r and B_s.

$$B_{rs} = B_r(\theta,t) + B_s(\theta,t)$$
$$= B_R \cos(\omega t - M\theta) + B_S \cos(\omega t - N\theta - \phi) \quad (3)$$

The control force can be generated by controlling imbalance of the magnetic flux distribution. The attractive force is expressed as the gradient of the magnetic energy. The magnetic flux energy in the air gap is given by equation (4),

$$W = \int_V \frac{B_{rs} H_{rs}}{2} dV = \int_0^{2\pi} \frac{{B_{rs}}^2}{2\mu_0} zrRd\theta \quad (4)$$

where H_{rs} is magnetic field intensity in the air gap, z and r are axial height and radial thickness of the air gap, R is length between the coordinate center and the center of the air gap. Therefore, the attractive force inside of the stator and rotor which is the gradient of the magnetic energy in the normal direction is given by equation (5).

$$F_r = \frac{dW}{dr} = \int_0^{2\pi} \frac{{B_{rs}}^2}{2\mu_0} zRd\theta \quad (5)$$

The x-directional force F_x is calculated by integrating the x component of the attractive force.

$$\begin{aligned} F_x &= \frac{zR}{2\mu_0}\int_0^{2\pi} {B_{rs}}^2 \cos(\theta)d\theta \\ &= \frac{zR}{2\mu_0}\int_0^{2\pi} [B_R \cos(\omega t - M\theta) \\ &\quad + B_S \cos(\omega t - N\theta - \phi)]^2 \cos(\theta)d\theta \\ &= \frac{B_R B_S zR}{4\mu_0}\int_0^{2\pi} \{\cos[(N-M+1)\theta + \phi] \\ &\quad + \cos[(N-M-1)\theta + \phi]\}d\theta \end{aligned} \quad (6)$$

This calculation produces a constant force when $N - M = \pm 1$.

$$F_x = \frac{B_R B_S zR\pi}{2\mu_0}\cos(\phi) \quad (7)$$

The y-directional force F_y when $N - M = \pm 1$ is similarly obtained as follows,

$$F_y = \frac{B_R B_S zR\pi}{2\mu_0}\sin(\phi) \quad (8)$$

The control force F_r is expressed the square root of sum of squares of F_x and F_y and is given by equation (9).

$$F_r = \sqrt{{F_x}^2 + {F_y}^2} \quad (9)$$

Hence, two dimensional radial position of the rotor can be controlled by changing the B_S and ϕ.

C. *Hydrodynamic bearing*

The hydrodynamic bearing was designed to avoid impeller touchdown when the levitated impeller received a large disturbance. Fig. 4 shows a schematic of the hydrodynamic bearing. A load carrying capacity Q was calculated to determine dimensions of the hydrodynamic bearing [4] by equation (10).

$$Q = \frac{3\pi}{2} g_1 \left(\frac{r_{eff}}{r_2}\right)^4 \left\{ \left[1 - \left(\frac{r_2}{r_{2eff}}\right)^2\right]^2 - 2\left[1 - \left(\frac{r_2}{r_{2eff}}\right)^2\right] \frac{A}{\left(In\frac{r_b}{r_1}\right)g_5 - \left(In\frac{r_2}{r_{2eff}}\right)g_3} \right\} \frac{\mu\omega {r_2}^4}{{h_2}^2} \quad (10)$$

where, r_1 is the inner radius of the grooved part of the hydrodynamic bearing [m], r_2 is the outer radius of the grooved part of the hydrodynamic bearing [m], r_{2eff} is the effective outer radius [m], r_b is the radius in the middle of the contacting surfaces at which spiral grooving ends [m], μ is viscosity of a working fluid [Pa/s], ω is angular velocity of the hydrodynamic bearing [rad/s]. g_1, g_3, g_5, A and r_{2eff} in equation (10) are as follows,

$$g_1 = \frac{\gamma\left(\frac{h_2}{h_1}\right)^2\left[1-\left(\frac{h_2}{h_1}\right)\right]\left[1-\left(\frac{h_2}{h_1}\right)^3\right]\cot\alpha}{\left[1+\gamma\left(\frac{h_2}{h_1}\right)^3\right]\left[\gamma+\left(\frac{h_2}{h_1}\right)^3\right]+\left(\frac{h_2}{h_1}\right)^3(1+\gamma)^2\cot^2\alpha} \quad (11)$$

$$g_3 = \left(\frac{h_2}{h_1}\right)^3(1+\gamma)(1+\cot^2\alpha)(1+\gamma)^2 \quad (12)$$

$$g_5 = \left[1+\gamma\left(\frac{h_2}{h_1}\right)^3\right]\left[\gamma+\left(\frac{h_2}{h_1}\right)^3\right]+\left(\frac{h_2}{h_1}\right)^3(1+\gamma)^2\cot^2\alpha \quad (13)$$

$$A = \left[\frac{r_2}{r_{2eff}}In\frac{r_2}{r_{2eff}}+\frac{1}{2}-\frac{1}{2}\left(\frac{r_2}{r_{2eff}}\right)^2\right]g_3 \quad (14)$$
$$-\left[\frac{r_2}{r_{2eff}}In\left(\frac{r_b}{r_1}\right)-\frac{1}{2}\left(\frac{r_2}{r_{2eff}}\right)^2+\frac{1}{2}\frac{r_1^2}{r_{2eff}^2}\right]g_5$$
$$-\frac{\pi}{2k}\left(1-\frac{\alpha}{90}\right)(\tan\alpha)\frac{2}{1+\gamma}\frac{1-\left(\frac{h_2}{h_1}\right)^3}{1+\left(\frac{h_2}{h_1}\right)^3}F_{r2}$$

$$r_{2eff} = r_2 e \quad (15)$$

with

$$s_{r2} = \frac{1}{2}\left[1-\left(\frac{r_b}{r_1}\right)^2\right]\frac{\gamma\left(\frac{h_2}{h_1}\right)^3(\cot\alpha)(1+\gamma)\left(1-\frac{h_2}{h_1}\right)\left[1-\left(\frac{h_2}{h_1}\right)^3\right]}{In\left(\frac{r_b}{r_1}\right)g_5-\left[In\left(\frac{r_b}{r_1}\right)\right]g_3} \quad (16)$$

$$F_{r2} = \left\langle 1+\frac{\gamma\left(\frac{h_2}{h_1}\right)^3(\cot\alpha)(1+\gamma)\left(1-\frac{h_2}{h_1}\right)+S_{r2}\left\{\left[\gamma+\left(\frac{h_2}{h_1}\right)^3\right]+\left(\frac{h_2}{h_1}\right)^3(\cot^2\alpha)(1+\gamma)\right\}}{-\gamma(\cot\alpha)\left[1-\left(\frac{h_2}{h_1}\right)\right]\left[1+\gamma\left(\frac{h_2}{h_1}\right)^3\right]+S_{r2}\gamma(\cot^2\alpha)\left[1-\left(\frac{h_2}{h_1}\right)^3\right]}\right\rangle^{-1} \quad (17)$$

where, h_1 is groove depth $H_g + h_2$ [m], h_2 is film height above the ridges [m], γ is ratio of ridge width a_2 divided by groove width a_1, α is groove angle.

The maximum load carrying capacity was calculated as 2.2 N with a bearing clearance of 10 μm, when a rotational speed of the impeller is 2,000 rpm and a viscosity of a fluid is 1 mPa·s. Groove depth, groove angle and ratio of ridge width to groove width were determined as 55 μm, 7 degrees and 1.0.

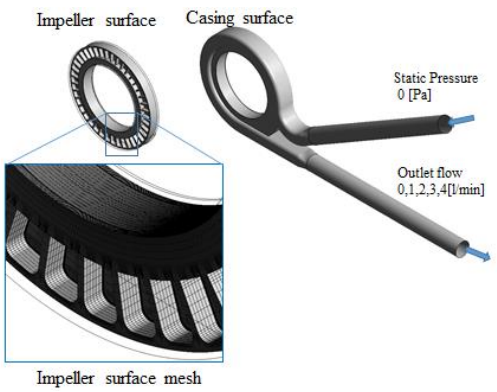

Figure 6. CFD Analysis model and mesh model.

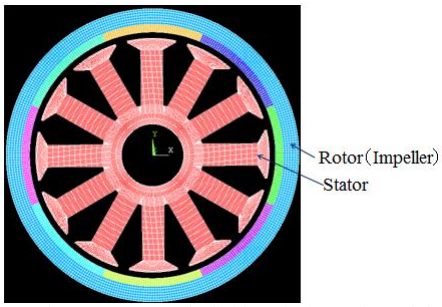

Figure 7. Magnetic field analysis mesh model.

III. EXPERIMENTS

A. CFD analysis

The CFD analysis was conducted to estimate the hydrodynamic force acting on the levitated impeller in order to determine the passive stability performance required to suppress the axial movement of the levitated impeller caused by the fluid force. Fig. 6 shows CFD analysis model and impeller surface mesh model. The analysis was carried out in the steady-state analysis by using the frozen rotor method with ANSYS CFX 14.0. Shear stress transport model has been adopted as a turbulent flow model. The working fluid is water which has density ρ = 997 kg/m^3, viscosity μ = 0.8899 × 10^{-3} Pa·s. Fluid forces with different mass flow rate condition from 0 L/min to 4 L/min were calculated with a rotating speed of 2,000 rpm. Fluid forces were calculated by integrating the force caused by the pressure and the wall shear stress of each mesh. Number of elements in the CFD analysis model is about 10 million.

B. Magnetic field analysis

The magnetic field analysis was performed to evaluate the restoring torque generated on the impeller with passive stability. The restoring force in the axial direction generated by the axial impeller displacement and the restoring torque generated by the inclination of the levitated impeller were calculated with the magnetic field analysis with ANSYS 14.0. Fig.7 shows the magnetic field analysis mesh model. The material of the permanent magnets is the Samarium-Cobalt (magnetic coercive force is 748 kA/m, remanent magnetic flux density is 1.02 T). The material of the impeller yoke and the stator yoke are magnetic steel (SUY-1) and laminated silicon steel (35A440), respectively. The position in the axial direction of the impeller was changed from 0 mm at the center position to 0.4 mm. The impeller inclination around Y axis was changed from 0 degree to 1.2 degrees. Number of elements in the magnetic field analysis model is about 1.2 million.

C. Hydrodynamic bearing performance

Fig. 8 shows the developed hydrodynamic bearing. The hydrodynamic bearing is formed on the rotor yoke's end face of the levitated impeller. The performance evaluation equipment of the hydrodynamic bearing was shown in Fig. 9 and 10. The stator of the self-bearing motor was set at the center of the equipment. A ring shaped permanent magnet

which gives a preload of 2.1 N in the axial direction on the levitated impeller is set on the axially movable stage under the rotated impeller. Glycerin-water solutions with a viscosity of 0.1 Pa・s was filled in the channel and the impeller was set in the channel and was immersed in the glycerin-water solution. The radial impeller position was controlled at the center and rotated with an axial preload by the self-bearing motor. At first, the impeller is set in the channel on the bottom. The rotational speed of the impeller increased gradually, the axial impeller position which is lifted off with hydrodynamic force was measured by using four eddy current sensors.

D. Prototype pump and pump performance

Fig. 11 shows the prototype pump of the maglev cascade VAD. The outer diameter and the axial thickness of the maglev VAD are 59 mm and 22 mm, respectively. The minimum clearances between the casing and the impeller in the radial and axial direction are 0.25 mm and 0.4 mm, respectively. The maximum tilt angle of the rotor is 1.2 degrees. Fig. 12 shows schematic of the radial type self-bearing motor's control system. Levitation and rotation of the rotor were controlled with a digital PID controller using a digital signal processor. Two eddy current sensors and three Hall elements are used to measure the rotor radial position and the rotation speed, respectively. Fig. 13 shows experimental set up for pump performance test. The pump performance, which is a relationship between the pump head and the flow rate, was evaluated. The prototype pump was connected to a closed mock circuit filled with saline. The closed mock circuit is composed of two pressure gauge sensors, an electromagnetic flow meter, and a reservoir tank. The pump head is the difference pressure between the static pressure of the inlet port and the static pressure of the outlet port. The maximum oscillation amplitude and power consumption during pumping were measured by using eddy current sensors and the power meter.

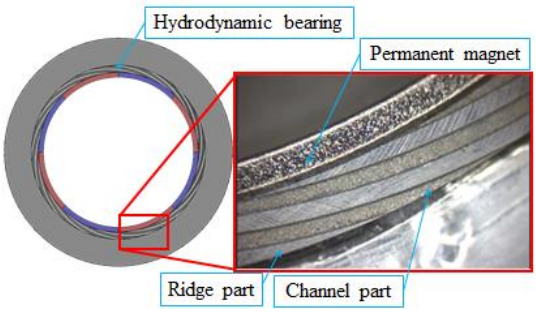

Figure 8. Developed hydrodynamic bearing.

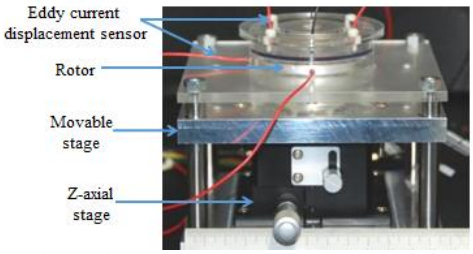

Figure 9. The performance evaluation equipment of the hydrodynamic bearing.

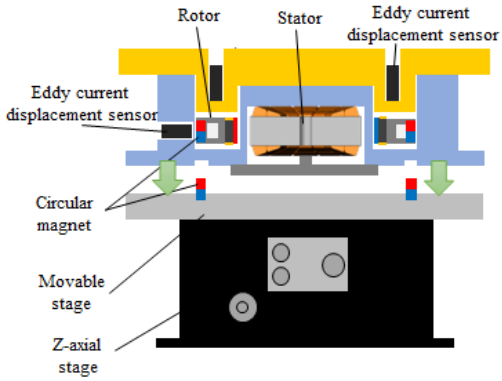

Figure 10. Schematic of the performance evaluation equipment of the hydrodynamic bearing.

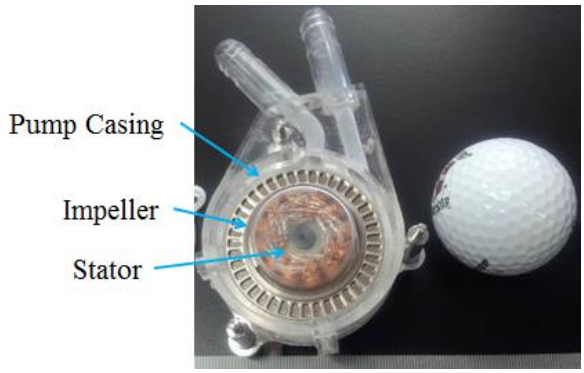

Figure 11. Prototype pump of maglev cascade VAD.

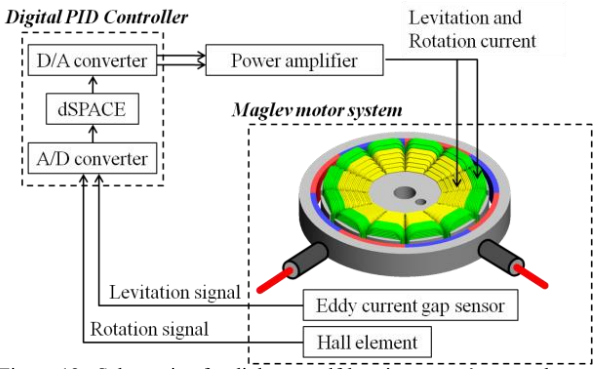

Figure 12. Schematic of radial type self-bearing motor's control system.

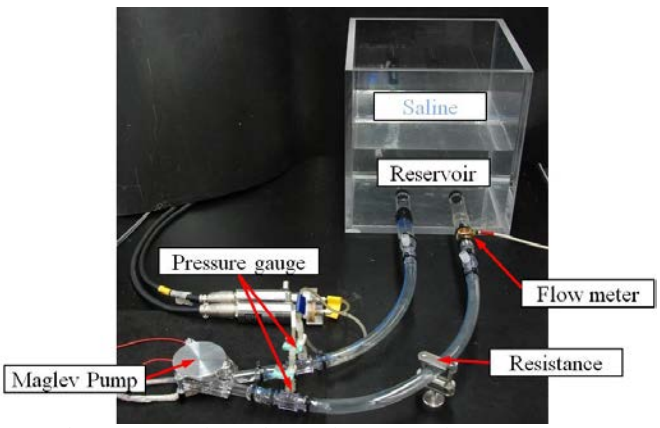

Figure 13. Experimental set up for pump performance test.

IV. RESULT

A. *CFD analysis*

Fig. 14 and 15 show hydrodynamic force in the axial direction and torque around Y axis corresponding to flow rate with a rotating speed of 2,000 rpm. Both of the axial hydrodynamic force and the torque around radial axis decreased with an increase in flow rate. The maximum axial hydrodynamic force was 0.16 N and the maximum torque around Y axis was 2.5 mNm at shutoff operation.

B. *Magnetic field analysis*

Fig. 16 and 17 show simulated restoring force in the axial direction and restoring torque around Y axis generated by the passive stability. The maximum restoring force in the axial direction was 1 N with a displacement of 0.4 mm. The restoring torque was 2.3 mNm with an inclination of 1.2 degrees.

C. *Hydrodynamic bearing performance*

Fig. 18 shows the relationship between the impeller axial position change and the rotating speed. The impeller was lifted off with the hydrodynamic effect when the rotating speed is over 1,000 rpm and the maximum levitated distance was 5 μm with a rotating speed of 3,000 rpm.

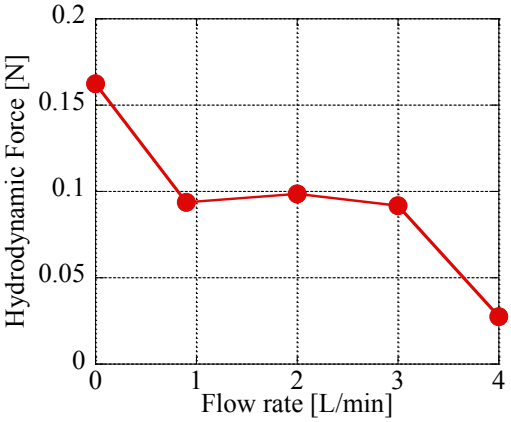

Figure 14. The relationship between the hydrodynamic force in the axial direction and flow rate calculated by the CFD analysis.

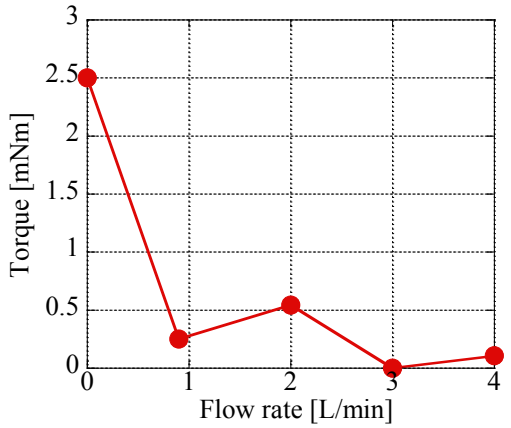

Figure 15. The relationship between the torque around the Y axis and flow rate calculated by the CFD analysis.

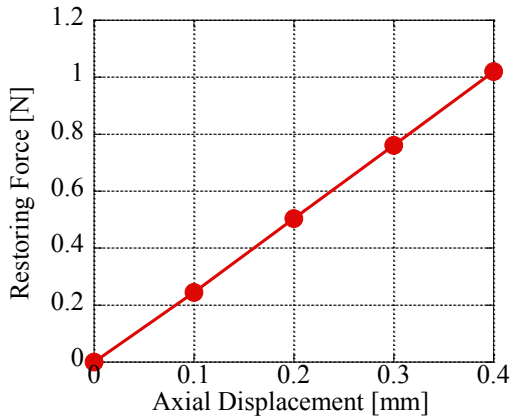

Figure 16. The relationship between the restoring force in the axial direction and the axial displacement of the rotor simulated by magnetic field analysis.

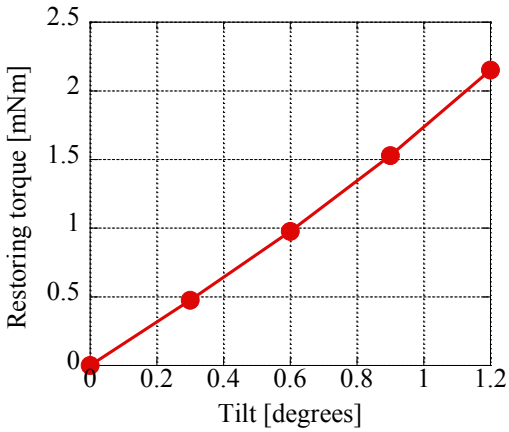

Figure 17. The relationship between the Y-axis restoring torque and the inclination of the rotor simulated by magnetic field analysis.

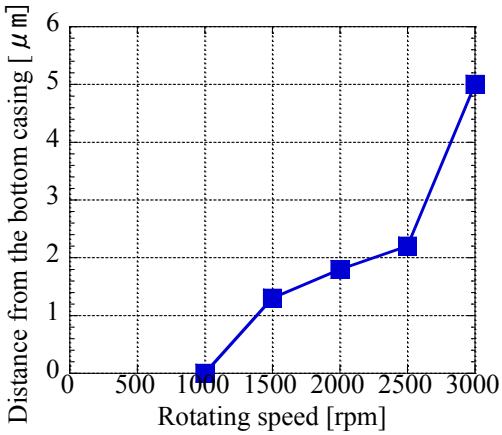

Figure 18. The relationship between the distance and the rotating speed of hydrodynamic bearing.

D. *Pump performance*

Fig. 19 shows the relationship between the pump head and the flow rate. Fig. 20 shows the relationship between maximum oscillation amplitude and the flow rate with different rotating speeds. The pump was levitated and rotated up to a rotating speed of 2,600 rpm successfully. The maximum head pressure and the maximum flow rate are 300 mmHg and 6.3 L/min.

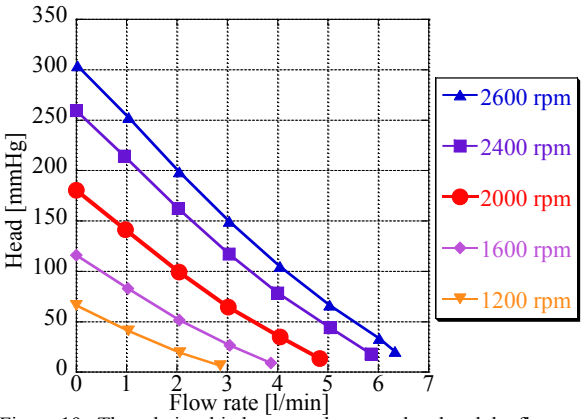

Figure 19. The relationship between the pump head and the flow rate.

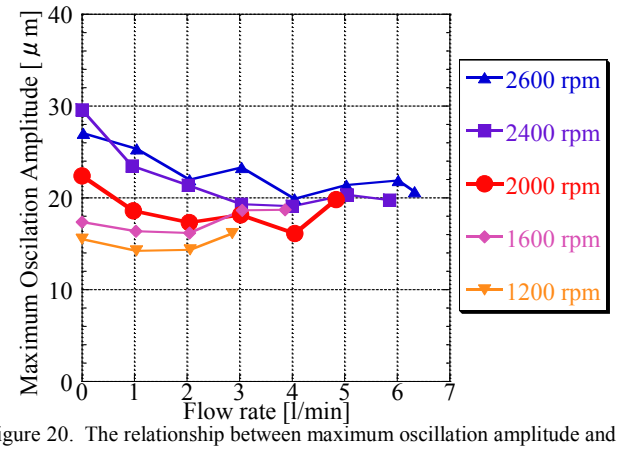

Figure 20. The relationship between maximum oscillation amplitude and the flow rate.

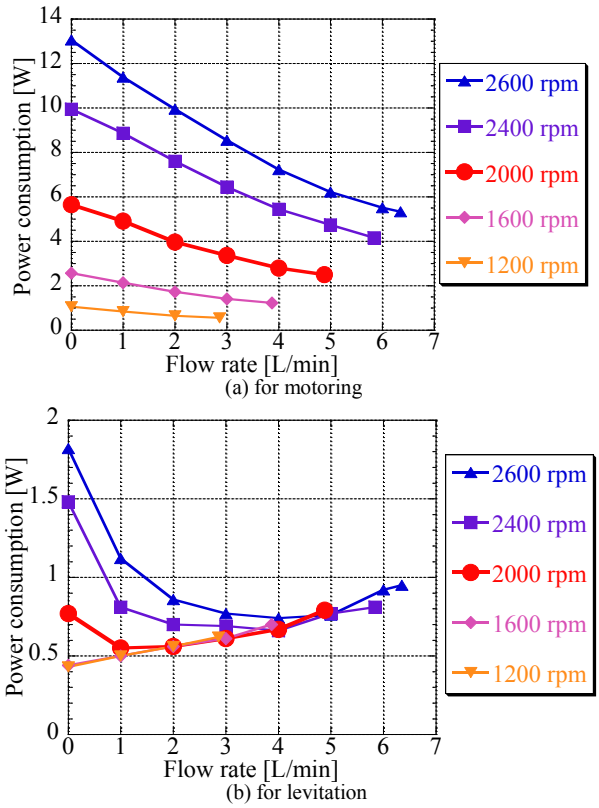

Figure 21. The relationship between the power consumption and the flow rate.

Fig. 21 shows the relationship between the power consumption and the flow rate. The maximum motor and levitation power consumption were 13 W and 1.8 W with a rotational speed of 2,600 rpm. The maximum oscillation amplitude of the levitated impeller is 30 μm with a rotating speed of 2,400 rpm. The target performance which is a flow rate of 2 L/min against a head pressure of 100 mmHg is achieved with a rotating speed of 2,000 rpm. The total power consumption and the maximum oscillation amplitude with the target performance were 4.5 W and 17 μm.

V. Discussion

The estimated axial fluid force by the CFD analysis was 0.01 N with a flow rate of 2 L/min and is smaller than an axial restoring force due to the passive stability that is 1 N estimated with the magnetic field analysis. The torque around the Y axis produced by the fluid force was 0.5 mNm and is also smaller than the maximum restoring torque by the passive stability which is 2.3 mNm. Therefore, the radial position and inclination of the levitated impeller is restricted by passive stability characteristics and it is also confirmed with the pumping experiment.

In the experiments of the hydrodynamic bearing, the levitated distance was 2 μm despite using glycerin-water solutions which has a viscosity of 0.1 Pa・s. The hydrodynamic bearing could produce lifting force to push the impeller away from the touchdown even the viscosity of the experimental working fluid is 10 times higher than the blood. The hydrodynamic bearing should be redesigned to enhance the lifting performance.

VI. Conclusion

A small, thin, maglev VAD, which can be implanted under the thorax muscle layer like a pacemaker, has been developed. A radial type self-bearing motor and a cascade pump are adopted to reduce the axial thickness of the device. The restoring force and toque produce by the passive stability in the uncontrolled axis were calculated by the magnetic field analysis and these are larger enough to restrict the levitated impeller posture compared with the fluid force which acts on the levitated impeller and was estimated by the CFD analysis. A developed hydrodynamic bearing to avoid touchdown of the impeller indicated the lift-off performance with higher viscous fluid. A prototype maglev pump indicated sufficient levitation performance and pump performance as a VAD.

References

[1] Eric A.Rose , “Long-term use of a left ventricure assist device for end-stage heart failure” , *The New England Journal of Medicine* , Vol.345,2001.11.

[2] K. Ukita, T. Masuzawa, H. Onuma, T. Nishimura, and S. Kyo, “A Radial Type Self-Bearing Motor for Small Maglev Regenerative Blood Pump “, Journal of the Japan Society of Applied Electromagnetics and Mechanics,Vol. 20, No. 2, pp. 312-318, 2012.

[3] H. Onuma, T. Masuzawa, K. Matsuda, and Y. Okada, “Magnetically levitated centrifugal blood pump with radially suspend self-bearing motor”, Proc. 8th International Symposium on Magnetic Bearings, pp. 3-8, 2002.

[4] E.A.Muijderman, “SPAIRAL GROOVE BEARINGS”, *Philips technical*, 1996.